GA–A24522

SUPPRESSION OF LARGE EDGE LOCALIZED MODES IN HIGH CONFINEMENT DIII–D PLASMAS WITH A STOCHASTIC MAGNETIC BOUNDARY

by
T.E. EVANS, R.A. MOYER, P.R. THOMAS, J.G. WATKINS, T.H. OSBORNE,
J.A. BOEDO, M.E. FENSTERMACHER, K.H. FINKEN, R.J. GROEBNER,
M. GROTH, J.H. HARRIS, R.J. LAHAYE, C.J. LASNIER, S. MASUZAKI,
N. OHYABU, D. PRETTY, T.L. RHODES, H. REIMERDES,
D.L. RUDAKOV, M.J. SCHAFFER, G. WANG, AND L. ZENG

NOVEMBER 2003

DISCLAIMER

GA–A24522

SUPPRESSION OF LARGE EDGE LOCALIZED MODES IN HIGH CONFINEMENT DIII–D PLASMAS WITH A STOCHASTIC MAGNETIC BOUNDARY

by
T.E. EVANS, R.A. MOYER,* P.R. THOMAS,† J.G. WATKINS,‡ T.H. OSBORNE, J.A. BOEDO,* M.E. FENSTERMACHER,◊ K.H. FINKEN,¶ R.J. GROEBNER, M. GROTH,◊ J.H. HARRIS,§ R.J. LAHAYE, C.J. LASNIER,◊ S. MASUZAKI,∞ N. OHYABU,∞ D. PRETTY,§ T.L. RHODES,£ H. REIMERDES,ø D.L. RUDAKOV,* M.J. SCHAFFER, G. WANG,£ AND L. ZENG£

This is a preprint of a paper to be submitted for publication in *Phyical Review Letters.*

*University of California San Diego, La Jolla, California
†CEA Cadarache Euratom Association, Cadarache, France
‡Sandia National Laboratory, Albuquerque, New Mexico
◊Lawerence Livermore National Laboratory, Livermore, California
¶FZ-Jülich Euratom Association, Jülich, Germany
§Australian National University, Canberra, Australia
∞National Institute for Fusion Science, Gifu-ken, Japan
£University of California, Los Angeles, California
øColumbia University, New York, New York

Work supported by
the U.S. Department of Energy under
Contract Nos. DE-AC03-99ER54463, DE-AC04-94AL85000,
W-7405-ENG-48 and Grant Nos. DE-FG03-95ER54294,
DE-FG03-01ER54615, DE-FG02-89ER53297

GA PROJECT 30033
NOVEMBER 2003

ABSTRACT

A stochastic magnetic boundary, produced by an externally applied edge resonant magnetic perturbation, is used to suppress large edge localized modes (ELMs) in high confinement (H–mode) plasmas. The resulting H–mode displays rapid, small oscillations with a bursty character modulated by a coherent 130 Hz envelope. The H–mode transport barrier is unaffected by the stochastic boundary. The core confinement of these discharges is unaffected, despite a three-fold drop in the toroidal rotation in the plasma core. These results demonstrate that stochastic boundaries are compatible with H–modes and may be attractive for ELM control in next-step burning fusion tokamaks.

The physics of complex stochastic magnetic field configurations has significant implications for research in astrophysical [1], solar [2], planetary [3] and laboratory [4] plasmas. In addition, studies of the structure of stochastic magnetic fields in tokamaks are yielding interesting new insights into the role of complex dynamical objects such as homoclinic tangles and Hamiltonian chaos [5] in toroidal plasma confinement devices.

In laboratory plasmas at the conditions necessary for controlled thermonuclear fusion, the tight coupling between the fusion power produced and the plasma edge conditions (the height of the H–mode pedestal) leads to requirements for high edge pressure gradients that generally produce large, repetitive heat and particle loading to the divertor targets known as "edge localized modes" (ELMs) [6]. These ELMs are governed by the details of the edge magnetohydrodynamic (MHD) stability, limit the core plasma performance, and reduce the divertor target plate lifetime due to increased erosion from the impulsive heat and particle fluxes [7]. However, the ELMs transport heat and particles outward across the boundary and thus allow for steady-state, high performance operating scenarios with density control and reduced core impurity content. Consequently, any technique to eliminate large fast ELM impulses while maintaining high H–mode edge pedestal conditions must replace the ELM-induced heat and particle transport with another, less transient, transport process. Such a technique would be highly desirable for a burning plasma experiment such as the proposed ITER device. A static stochastic boundary might provide a method for reducing large, fast ELM impulses by limiting the edge pedestal conditions while replacing the ELM transport with steady-state transport along the stochastic magnetic field lines. While stochastic magnetic layers have been studied under a variety of laboratory plasma conditions [4] these studies have been entirely missing in high confinement (H–mode) poloidally diverted tokamak plasmas with large ELMs. In this paper, we report the first such experiments and highlight results showing that large ELMs can be suppressed with a stochastic boundary layer without degrading the quality of the H–mode confinement regime.

Steady-state H–mode plasmas without large amplitude ELMs have been produced in the DIII–D tokamak by applying small resonant magnetic field perturbations. In these plasmas, applied perturbations with amplitudes less than 0.25% of the equilibrium field result in the conversion of large amplitude ELMs, seen in the particle recycling signals, into small amplitude intermittent bursts modulated by a coherent 130 Hz periodic oscillation. Simultaneously, the edge toroidal rotation drops to zero or reverses and the core toroidal rotation is reduced by at least a factor of 3 with no degradation in the stored energy or the energy confinement. The H–mode radial transport barrier is not affected by the magnetic perturbations, and electron pedestal profiles are not significantly changed. These results demonstrate that stochastic boundary layers are compatible with high quality H–mode plasma regimes and that a stochastic layer can suppress ELMs without degrading the global particle and energy confinement of the plasma.

The magnetic perturbations applied in this experiment are produced by a set of control coils, referred to as the I–coil, located inside the vacuum vessel [8]. The DIII–D error field correction coil (C–coil) was not used in this experiment, since, in addition to attempting to correct a known field error at the q = 2 surface, it also perturbs the boundary [9]. As shown in this letter, intrinsic field errors, common to most tokamaks, also play a role in the edge perturbations and, in general, have a different phase and symmetry than that of the applied magnetic perturbation. On DIII–D, their effects are seen when the applied perturbation from the I–coil is rotated toroidally by 60° in otherwise identical discharges and the behavior of the edge changes significantly.

A small nonaxisymmetric magnetic perturbation from the I–coil is switched on during the discharge by a dc current of 4.4 kA in each of the 12 single-turn loops comprising the coil, six above and six below the midplane. The individual loops are constructed in a window pane geometry and are mounted behind protective graphite tiles on the low field side of the vessel. The loops are up-down symmetric with respect to the midplane at each toroidal angle. For the experiments discussed here, both the upper and lower coil segments were configured for a toroidal mode number $n = 3$ and had opposite current polarities in the two loops at the same toroidal angle. This configuration results in an up-down asymmetric or odd parity perturbation.

TRIP3D modeling [9] of the I–coil perturbation, an example of which is shown in Fig. 1(a), indicates that a narrow poloidal flux (ψ) loss region, with a width $\Delta\psi_{fl} = 2.9\%$, is formed just inside the unperturbed separatrix along with a weakly stochastic zone containing remnant islands and field lines that randomly traverse small regions of unperturbed poloidal flux. The width of the stochastic region ($\Delta\psi_{slw}$) is seen to be $\Delta\psi_{slw} = 10.0\%$ from Fig. 1(a) for this discharge. Here, all the known sources of intrinsic field errors [10] are included in the modeling. In this mode of operation, the modeling indicates that the I–coil has relatively little effect on core resonances other than producing small $n = 3$ islands (no larger than 2 cm or ~3% of the minor radius at the outer midplane) with poloidal mode numbers m between 3 and 6. The unperturbed discharge shape is shown in Fig. 1(b) where the shaded boundary region corresponds to the TRIP3D computational domain in Fig. 1(a).

The plasmas used in this experiment were primarily double null diverted (DND) discharges that were magnetically unbalanced downward by 2 cm [Fig. 1(b)] to take advantage of an extensive array of lower divertor diagnostics. The discharges had a major radius (R_0) of 1.722 m with a minor radius (a) at the outer midplane of 0.585 m. The elongation (κ) was 1.8 with upper and lower triangularities of 0.35 and 0.73, respectively. The toroidal magnetic field $B_T = 1.6$ T, the plasma current $I_p = 1.1$ MA, and the neutral beam heating power of $P_{inj} = 5.1$ MW while the safety factor at the 95% flux surface $q_{95} \approx 3.7$. The time history for a typical discharge with ELM suppression is compared to a reference discharge that was identical except for the absence of the I–coil pulse and concomitant ELM suppression in Fig. 2. The electron pedestal density normalized to the Greenwald density [11] was 0.55 with a line average density of 7.2×10^{19} m^{-3} [Fig. 2(b)]. These discharges typically went into H–mode at about 1600 ms and established regular type-I ELMs within 300 to 400 ms after the L–H transition [Figs. 2(c) and (d)]. Prior to

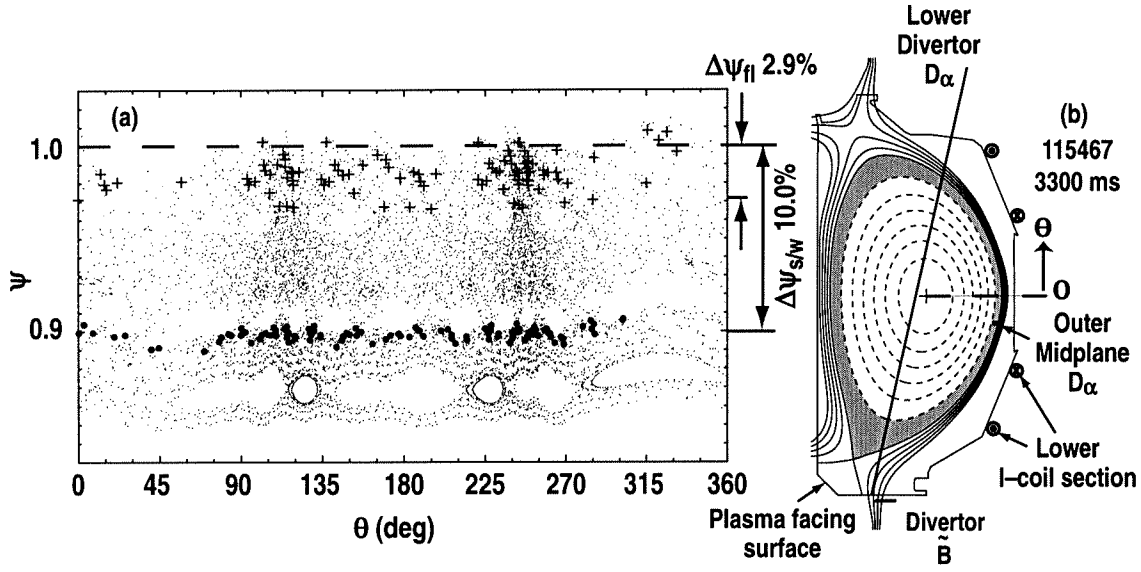

Fig. 1. (a) Poincaré plot of the edge vacuum magnetic field line topology in the (ψ,θ) plane calculated by TRIP3D using the known intrinsic field errors and an n = 3, 4.4 kA odd parity I–coil perturbation with 0° toroidal phase. Here, ψ is the normalized poloidal magnetic flux (a radial coordinate) and θ is the poloidal angle indicated in (b). The unperturbed separatrix is indicated with a dashed line at ψ = 1. The black "+" symbols in the region 0.97 < ψ < 1 show the trajectory intersections of the innermost magnetic field line which is lost by crossing the separatrix into the region ψ > 1. The black "•" symbols near ψ = 0.9 highlight the trajectory of the innermost magnetic field line which is stochastic without being lost from the plasma. (b) The unperturbed equilibrium reconstruction from the EFIT Grad-Shafranov solver showing ψ contours (dashed ovals) and the TRIP3D computational domain of (a) as a shaded region at the edge of the plasma.

switching on the I–coil, the properties of these plasmas are typical of those found in standard DND ELMing H–modes. Large type-I ELMs are seen on all the D_α channels (midplane, inner wall, and upper and lower divertors), on the divertor floor and midplane reciprocating Langmuir probes, on the fast magnetic signals and on the midplane reflectometers.

Within one ELM cycle (about 15 ms) after switching on the I–coil at t = 3000 ms [Fig. 2(a)], the large type-I ELM behavior seen on the D_α signals is substantially reduced except for a few isolated events [Fig. 2(d)]. The ELM behavior in the reference discharge, without I–coil current, is shown in Fig. 2(c) for comparison. Throughout the I–coil pulse and ELM suppression, the discharge remains in H–mode and the core confinement, as indicated by the plasma stored energy [Fig. 2(e)], remains nearly constant. The application of the edge resonant magnetic perturbation from the I–coil also splits the profile of the heat flux at the divertor target plate, leading to a reduction in the peak heat flux averaged over ELMs by spreading the heat flux over a large area of the divertor target [Fig. 2(f)]. This reduction in the peak heat flux near the strike point is correlated with the I–coil pulse and confirms that the applied I–coil perturbation is sufficient to alter the edge magnetic topology [5].

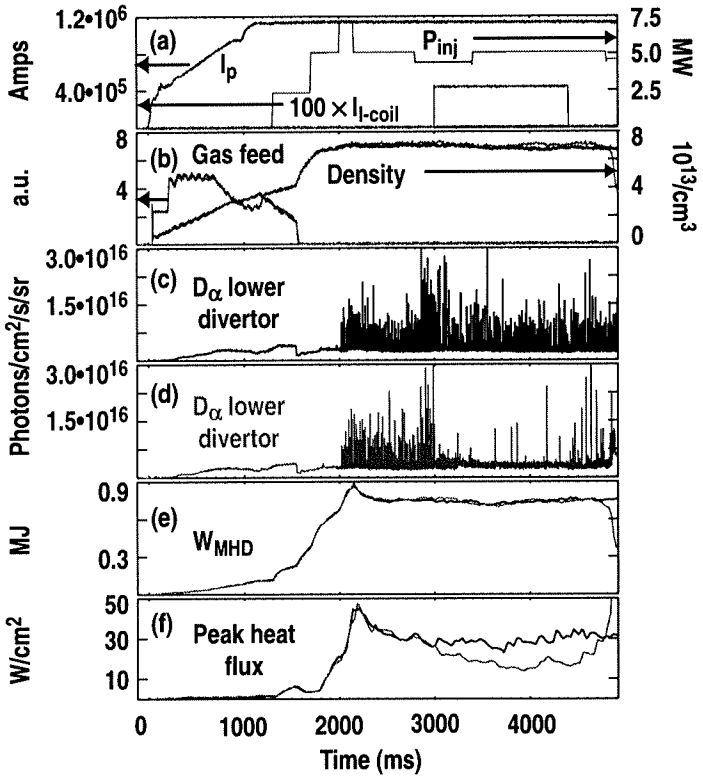

Fig. 2. (a) Plasma current, injected neutral beam power P_{inj}, and I–coil pulse are shown for two identical discharges with (115467: red) and without (115468: black) I–coil current. The gas puff and line integrated electron density (b) are seen to be identical with and without the I–coil while the ELM behavior (c) is significantly different in the discharge with the I–coil (d). Shown in parts (e) and (f) are the stored energy and peak heat flux in the lower divertor respectively with (red) and without (black) the I–coil.

The suppression of the impulses due to type-I ELMs is seen globally on all the recycling and other diagnostics used to monitor the ELM properties as shown in the expanded view of Fig. 3. The prompt suppression of the ELMs is seen in the D_α signals monitoring the outboard midplane [Fig. 3(a)] and the lower (primary) divertor [Fig. 3(b)], in the particle flux to the divertor target plate, measured by fixed Langmuir probes near the divertor strike point [Fig. 3(c)], and in the surface temperature measured by an infrared TV camera in line-scan mode with a time resolution of 100 μsec [Fig. 3(d)]. In addition, there is a relatively slow ($\tau \approx 300$ ms) decay of the toroidal rotation [Fig. 3(e) black] compared to an identical reference discharge [Fig. 3(e) gray]. In Fig. 3(f), a magnetic probe located near the strike point in the lower divertor records edge MHD fluctuations without contributions from the core MHD modes that dominate the midplane magnetic probe signals. Here we see an increase in the bursty fluctuation behavior with a low frequency (130 Hz) modulation that switches the fluctuations on and off. A similar behavior is seen in the density fluctuations measured by the midplane reflectometers and in the particle flux measured by a reciprocating Langmuir probe array on the outer midplane several centimeters outside the unperturbed separatrix.

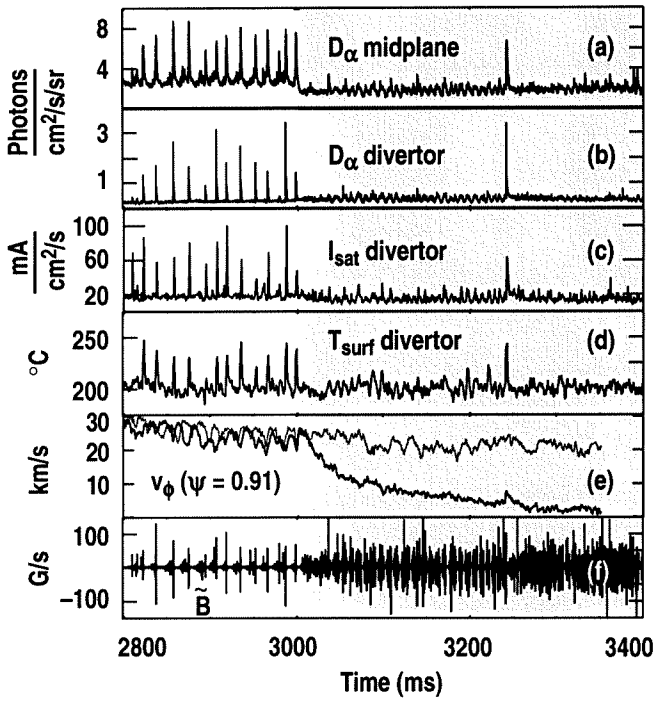

Fig. 3. ELM suppression during a discharge (115467) with a 4.4 kA odd parity $n = 3$ I–coil pulse starting at 3000 ms using the configuration shown in Fig. 1. The D_α recycling response from a midplane chord (a) and a lower divertor chord (b), are shown with the particle flux to a fixed Langmuir probe (c) and the surface temperature from an IR camera view (d) near the outer strike point in the lower divertor. The change in the toroidal rotation is shown in (e) with the I–coil perturbation (black) as compared to the reference discharge without the I–coil pulse (gray). Also shown are the lower divertor (f) magnetic fluctuation (Mirnov) signals showing changes in the magnetic fluctuations when the ELMs are suppressed. The shaded region indicates the time when the I–coil is pulsed on with a current of 4.4 kA.

The resonant character of the ELM suppression was verified in a set of discharges in which q_{95} was varied by ramping the plasma current during the I–coil pulse. Using discharges having the same parameters as those shown in Fig. 2, an odd parity I–coil pulse was triggered 300 ms before starting the q_{95} ramp. It was found that the ELM suppression was maximized for $3.5 \leq q_{95} \leq 4.0$. This indicates that the ELM suppression results from the pedestal plasma response to the resonant interaction of the applied perturbation with the equilibrium.

The core performance, when compared to an identical discharge without the I–coil perturbation, is unaffected by the I–coil pulse or ELM suppression as shown in Fig. 2. The plasma stored energy is unchanged [Fig. 2(e)], while both the normalized plasma pressure $\beta_N = \beta/I_p/aB = 2.2$ and the H–mode quality factor $H_{L89} = 2.1$ remain constant. In addition, the gas fueling rate drops to zero when the plasma transitions into H–mode [Fig. 2(b)] and remains zero throughout both the reference ELMing discharge and the discharge with the ELMs suppressed. The total power radiated from the plasma core is also unaffected by the I–coil pulse. Since the plasma reaches a similar steady state with the same input power but without the impulsive particle and heat transport associated with the ELMs, the average radial transport during the I–coil pulse must be near the level obtained in the ELMing phase. Measurements show that the

broadband magnetic field, density, and potential fluctuation levels increase during the ELM suppression phase indicating that the impulsive transport associated with the ELMs may be replaced in part by a more steady turbulent transport in conjunction with parallel transport along the stochastic field lines.

A detailed analysis of the pedestal profiles shows that the H–mode pedestal height and radial transport barrier are unchanged during the I–coil pulse. A small ($\delta\psi$ = 1.5%) outward shift in the time average pedestal electron pressure is seen during the I–coil pulse, as indicated by the black squares and dashed line relative to the circles and solid gray line in Fig. 4(a). The ion channel, however, shows some changes that may be important for the edge stability, including an increase

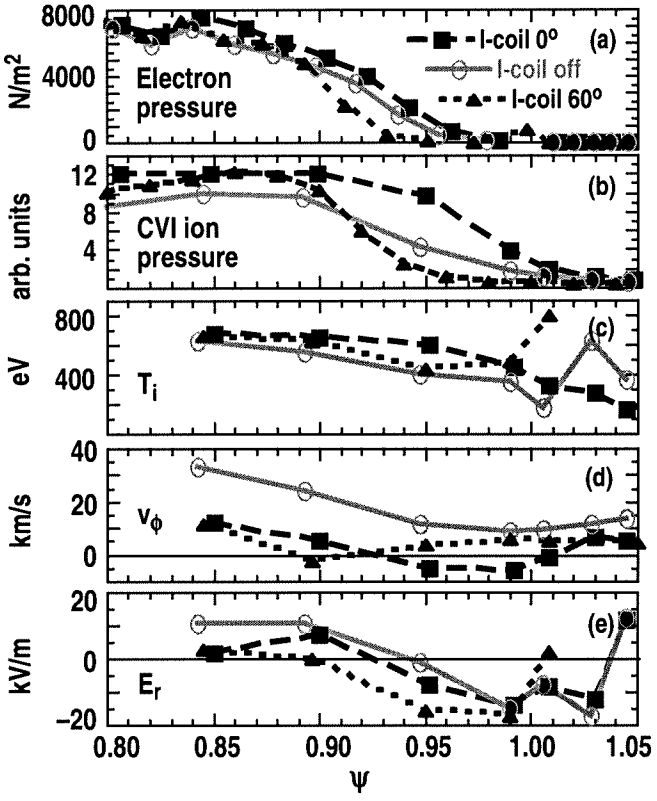

Fig. 4. Electron pressure P_e (a), CVI pressure profile P_{CVI} (b), ion temperature $T_{CVI} \approx T_i$ (c), toroidal rotation v_ϕ (d) and radial electric field E_r (e) with (black dashed lines) and without (gray solid lines) the I–coil perturbation. The reference discharge (circles/gray line) and two discharges with I–coil pulses having 0° toroidal phase (filled squares; good ELM suppression as in Figs. 2 and 3) and 60° toroidal phase (filled triangles; less ELM suppression as in Fig. 5) are shown.

in the pedestal carbon VI (CVI) ion pressure during the I–coil pulse [Fig. 4(b)] as measured with charge exchange recombination spectroscopy. There is a similar broadening in the ion temperature T_i [Fig. 4(c)] in the pedestal, suggesting that the main ion pressure profile also increases. The plasma size changes are deduced from parameterization of the distance between the vessel wall and the separatrix at the inner and outer midplanes ("inner" and "outer" gaps)

from fast equilibrium reconstructions. The edge toroidal rotation [Fig. 4(d)] decreases across the pedestal and reverses direction in the region where the carbon VI impurity pressure is increased with little or no change in the carbon VI poloidal rotation (not shown). The radial electric field E_r [Fig. 4(e)] is unchanged.

Prior to the I–coil pulse, the plasma is in a conventional type-I ELMing H–mode with $2p'_e$ well above the infinite-n ideal ballooning limit and $2p'_e$ remains well above the ballooning limit during the I–coil pulse as indicated by the profiles in Fig. 4(a). However, the carbon and deuterium ion temperature as well as the carbon VI density increase in the boundary which may change the bootstrap current, for example, due to an increase in the effective ion charge Z_{eff} in the boundary. A careful stability analysis is underway to clarify these important points.

The 130 Hz oscillations seen on the particle flux [Fig. 3(c)] and recycling signals [Figs. 3(a) and 3(b)] during the I–coil pulse correlate with a periodic 1 to 2 ms expansion of the plasma during the low recycling phase followed by a 6 ms contraction of the plasma where the recycling increases. The recycling signals become significantly more bursty in character during the contraction phase of the cycle. Based on the changes in outer midplane separation with the wall, the amplitude of the oscillation is about 0.9% in ψ and is a global effect that is in phase on all the recycling signals. There is a corresponding decrease in plasma stored energy of 5 to 15 kJ during each contraction, compared to a stored energy loss of 15 to 20 kJ during each of the shorter type-I ELM impulsive spikes. The nature of these oscillations, while lower in amplitude and about a factor of three longer in time, is similar to that seen during the type-I ELMs prior to the I–coil pulse in the discharge. Thus, during the I–coil pulse, it appears that the plasma has established a new dynamical state in which the integrated transport during one cycle of these oscillations is roughly equivalent to that during a single type-I ELM spike but over an extended time and without the large impulses characteristic of the type-I ELMs.

The phase of the I–coil perturbation was rotated 60° toroidally in an identical discharge while maintaining the same current amplitude and parity in order to determine if intrinsic field errors play a significant role in the suppression of the large ELMs. In contrast to the 0° toroidal phase case, the 60° phase I–coil pulse resulted in a somewhat less effective ELM suppression [more large amplitude "ELMs" remained, cf. Fig. 5(b)], although the suppression is still quite significant. In the 60° case, the oscillations present during the 0° I–coil pulse were not observed, and the structure of the magnetic signal in the divertor [Fig. 5(c)] was significantly different. The H–mode pedestal response to the perturbation was also quite different: the edge electron pressure dropped just inside the separatrix [dashed black line in Fig. 4(a)] while the pressure at the top of the pedestal near $\psi = 0.9$ remained constant. The time-dependent evolution of the electron pressure for the 0° and 60° cases, given in Figs. 5(d) and 5(e), respectively, show an increase on all four channels spanning the pedestal with the 0° phasing and a strong decrease on the corresponding channels with the 60° phasing. These are consistent with the time averaged profiles shown in Figs. 4(a) and 4(b) and suggest a small $\delta\psi = 1.5\%$ outward shift in the pedestal profile for the 0° phasing and a larger $\delta\psi = 5\%$ inward shift for the 60° phasing. Because the ion

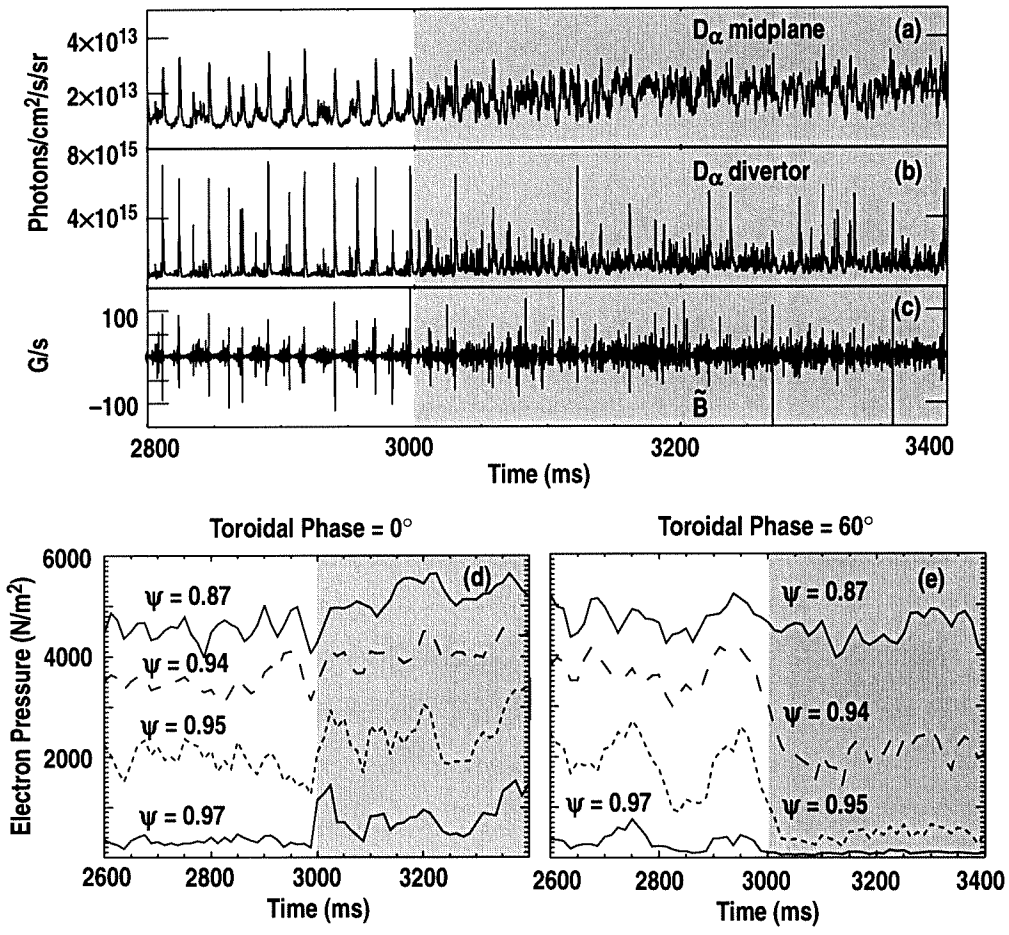

Fig. 5. Midplane recycling signal (a), lower divertor recycling signal (b), and an edge magnetic fluctuation signal (c) during a discharge with the toroidal phase of the I–coil perturbation rotated 60° with respect to the phasing used in the ELM suppression discharge in Figs. 2 and 3. The electron pressure as measured by the Thomson scattering chords in the pedestal increases with 0° phasing (d) and decreases for 60° phasing (e). The shaded regions indicate when the I–coil is on with a current of 4.4 kA.

and electron pressure profiles are measured at different toroidal and poloidal locations, these results suggest that the difference in the response is a global effect and that a substantially different stochastic boundary structure exists for these two cases. The ion pressure [Fig. 4(b)] is also substantially different in the 60° case compared to the 0° case and small differences are seen in the ion temperature [Fig. 4(c)], toroidal rotation [Fig. 4(d)] and radial electric field [Fig. 4(e)] for these two cases. In addition, during the 60° case the overall recycling level between ELMs measured at the outer midplane [Fig. 5(a)] increased until individual ELM events were no longer distinguishable on any of the eight chords with tangential views spanning the outer midplane. The complete elimination of apparent ELM events on all the midplane recycling measurements, in conjunction with a significant reduction in the frequency and amplitude of ELMs as seen in the divertor [Figs. 5(b) and 5(c)], are suggestive of the behavior reported for the enhanced D_α (EDA) mode of operation in the C–Mod tokamak, another type-I ELM-free mode of tokamak

operation [12]. A possible interpretation is that the intrinsic field errors, due to coil misalignments, bus bars, etc., or even due to the magnetic field of the quasi-coherent (QC) mode, might produce a stochastic layer in C–Mod sufficient to contribute to ELM suppression.

As with the 0° toroidal phase case, no change in the core confinement was observed in the 60° case while the pedestal profiles showed a significantly different response to the perturbation from the I–coil (i.e., instead of moving the pressure gradient outward by ~1.5% in poloidal magnetic flux it moved inward by ~5%). The effect of the I–coil perturbation during the 60° toroidal phase shift case is consistent with a broader stochastic layer compared to discharges with no toroidal phase shift. It is possible that a toroidal asymmetry, induced by a stationary helical mode in the pedestal region (i.e., a remnant magnetic island) that moves when the I–coil perturbation is rotated, could explain these differences. However, the observations are more consistent with a broadening of the flux loss region that could be explained by the existence of an unknown "field error" that mixes differently with the two phases of the I–coil perturbation. In contrast, modeling of these discharges with the TRIP3D code, using all the known error fields, predicts that the stochastic boundary width $\Delta\psi_{slw}$ and flux loss region $\Delta\psi_{fl}$ are slightly thinner with the 60° phasing than with the 0° phasing. These results indicate that additional field error sources are present in DIII–D and alter the effectiveness of the ELM suppression.

In conclusion, large type-I ELMs have been suppressed by applying an edge magnetic perturbation to produce a weakly stochastic boundary without affecting the core confinement or the H–mode transport barrier. The effectiveness of the magnetic perturbation in suppressing large ELMs depends on the value of q_{95} and on the toroidal phase of the applied perturbation. There is a relatively sharp window in q_{95} between 3.5 and 4.0 that is consistent with a resonant effect of the applied magnetic perturbation. A 60° change in the toroidal phase of the magnetic perturbation, in an otherwise identical discharge, produces a significantly different pedestal behavior. For the 0° phasing, large ELMs are strongly suppressed; while for the 60° phasing, it appears that the ELMs on the midplane are "covered up" by an increase in the baseline recycling similar to the behavior seen in an EDA H–mode on Alcator C–Mod. This result is consistent with the existence of other "intrinsic" field errors in the DIII–D device and suggests that these "field errors" play a role in the behavior of the ELMs seen in a particular machine. Because these field errors affect the magnetic topology in the pedestal region, understanding ELM stability and developing a predictive model for the H–mode pedestal will likely require some increased understanding of field error effects in future devices and the nature of the plasma response to them. Finally, the results presented here were obtained in double null discharges optimized for high performance Advanced Tokamak operations, a regime that is "close" to conditions (e.g., high triangularity) for achieving type-II ELMs in other devices [13]. It is not clear from these results whether the suppression of large type-I ELMs can also be achieved in low triangularity ITER-like shapes, or extended to higher power operating regimes. Future experiments in DIII–D will explore this possibility and may eventually result in a robust ELM suppression scenario for fusion reactors based on more conventional tokamak shapes such as ITER.

ACKNOWLEDGMENTS

This work was supported by the U.S. Department of Energy under Contract Nos. DE-AC03-99ER54463, DE-AC04-94AL85000, W-7405-ENG-48 and Grant Nos. DE-FG03-95ER54294, DE-FG03-01ER54615, DE-FG02-89ER54297.

REFERENCES

[1] B. J. Albright, Phys. Plasmas **6**, 4222 (1999).

[2] P. Mininni, D. Gómez, and B. Mindlin, Solar Phys. **201**, 203 (2001).

[3] F. Spahn, A. V. Krivov, M. Sremevi, U. Schwarz, and J. Kurths, J. Geophys. Res. **108**, 5021 (2003).

[4] Ph. Ghendrih, A. Grosman, and H. Caps, Plasma Phys. Control. Fusion **38**, 1653 (1996).

[5] R. K. W. Roeder, B. I. Rapoport, and T. E. Evans, Phys. Plasmas **10**, 3796 (2003).

[6] A. V. Loarte, *et al.*, Nucl. Fusion **44**, 733 (2002).

[7] G. Federici, *et al.*, J. Nucl. Mater. **266–269**, 109 (2003).

[8] G. L. Jackson, et al., *Proceedings of the 30th European Physical Society Conference on Controlled Fusion and Plasma Physics, St. Petersburg, 2003* (European Physical Society, Geneva 2003) CD–ROM, P-4.47.

[9] T. E. Evans, R. A. Moyer, P. Monat, Phys. Plasmas **9**, 4957 (2002).

[10] J. L. Luxon, *et al.*, "Anomalies in the Applied Magnetic Fields on DIII–D and their Implications for the Understanding of Stability Experiments," submitted to Nucl. Fusion (2003).

[11] M. Greenwald, *et al.*, Nucl. Fusion **28**, 2199 (1988).

[12] S. J. Wukitch, *et al.*, Phys. Plasmas **9**, 2149 (2002).

[13] J. Stober, *et al.*, Nucl. Fusion **41**, 1123 (2001).